Lab on a Chip

ARTICLE

Electrokinetic Energy Harvesting using Paper and Pencil

Sankha Shuvra Das[a], Shantimoy Kar[b]†, Tarique Anwar[a], Partha Saha[a] and Suman Chakraborty[ab]*

Received 00th January 20xx,
Accepted 00th January 20xx

DOI: 10.1039/x0xx00000x

www.rsc.org/

We exploit the combinatorial advantage of electrokinetics and tortutosity of cellulose-based paper network on a laboratory grade filter paper for the development of a simple, inexpensive, yet extremely robust (shows constant performance till 12 days) 'paper-and-pencil'-based device for energy harvesting application. We successfully achieve to harvest maximum output power of ~ 640 pW in single channel, while the same is significantly improved (by ~ 100 times) with the use of multichannel microfluidic array (maximum up to 20 channels). Furthermore, we also provide theoretical insights to the observed phenomenon and show that the experimentally predicted trends agree well with our theoretical calculations. Thus, we envisage that such ultra-low cost devices may turn out to be extremely useful in energizing analytical microdevices in resource limited settings, for instance for extreme point of care diagnostics applications.

Introduction

Throughout the last decade, paper-based microfluidics caught significant attention for myriad of applications[1–3], ranging from disease diagnostics[4–6], blood-plasma separation[7], water quality control[8], food quality monitoring[9] to heavy metal ion detection[10] . Recent studies show that paper-based microfluidic devices may also be used for probing fundamental phenomena like micro-mixing[11], electro-wetting[12], digital microfluidics[13] etc. In most of the scenarios, paper-based devices have been utilized for qualitative/semi-quantitative purposes and have been preferred because of their frugality, disposability, and easy manufacturing[14]. In recent years, paper-based devices have also been found suitable for energy storage applications e.g. flexible electronics, development of fuel cells etc[15–19].

Miniaturization of various bio-electronics and microfluidic-based lab-on-chip devices has essentially demand an integrated power source for powering those micro-chips. Towards this end, realizing an alternate source of green energy generation for these microfluidic chips is certainly one of the key concerns. To achieve this feat, many different mechanisms like solar cells[20], dye sensitized solar cells (DSSCs)[21], bio-mass conversion[22], microbial energy harvesting[23] etc. are extensively explored. Despite the inherent advantages of the aforesaid processes, all the underlying principles have certain limitations alike low conversion efficiency of ~9-13%, moderate to high fabrication cost, explicit dependence on substrate specificity (polymeric solar cells, ITO electrodes, porphyrin dyes, biomass, biocatalysts etc.). Moreover, such devices are not intrinsically designed to integrate other functionalities such as point of care medical diagnostics for on-field operations, in the same platform. In parallel, electrokinetic energy conversion mechanisms, mediated by the establishment of a streaming potential (i.e. the potential generated due to the continuous transport of electrolytes), has of late emerged to be as effective alternative[24]. Recent studies have successfully demonstrated the application of this paradigm, albeit in a sophistically controllable laboratory environment that cannot possibly be replicated for catering the functionalities of point of care devices in resource-limited settings[25–30]. In addition, the reported devices on electrokinetic energy conversion necessitate elaborate device fabrication, expensive consumables and trained personnel. Furthermore, these devices not only demand very intricate operational module, but also do not inherently integrate with low cost analytical platforms (such as paper strips); which eventually makes the entire paradigm expensive[31]. In the recent past, nano-porous membranes were utilized to generate streaming potential by applying a pressure gradient across them[32,33]. On such nano-porous membranes, it is seen that the conversion efficiency has improved significantly at the cost of consuming a considerable amount of input energy. Furthermore, there have been attempts to exploit the combinatorial effect of capillarity and associated evaporation towards exploiting electrokinetic energy generation in nano-porous membranes[34,35]. However, the sophisticated fabrication and surface treatment of such nano-porous membranes restricts their applications for empowering portable devices in inexpensive settings.

Comprehensive literature review shows that recent endeavors have been directed towards facilitating on-chip power generation. Meng *et al.* illustrated the concept of electrochemically induced CO_2 bubble driven liquid fuel cell which seems to be useful for continuous fluid flow[36]. However, the associated fabrication

[a] *Department of Mechanical Engineering, Indian Institute of Technology Kharagpur, Kharagpur 721302, India*
[b] *Advanced Technology Development Centre, Indian Institute of Technology Kharagpur, Kharagpur 721032, India. email: suman@mech.iitkgp.ernet.in*
†Currently working as a Postdoctoral Research Associate in Technische Universitat Darmstadt, Germany.
Electronic Supplementary Information (ESI) available: [details of any supplementary information available should be included here]. See DOI: 10.1039/x0xx00000x

difficulties and poor performance of the electrode restricts its utilitarian scope for continuous power generation. Arun *et al.* have demonstrated the usage of 'paper-and-pencil' based fuel cells for sustained period of power generation[37]. In such a system, graphite electrodes trap atmospheric oxygen and thus act as an internal source of oxygen. However, the process uses formic acid as a fuel and sulfuric acid as an oxidant which confine the scope of the device. Furthermore, performance enhancement of such devices (like microfluidic battery, triboelectric nanogenerators) requires a coating of different materials; hence, the efficiency is often constrained by the thickness of the adsorbed material[38–42].

In this work, we explore electrokinetics on a simple 'paper-and-pencil' based platform (shown in Figure 1) as a greener alternative for on-chip energy harvesting. The primary advantages of such a platform are the self-propelling nature of the input flow through an exploitation of intrinsic capillary transport in paper pores (to this end, no syringe pump or equivalent actuation is necessary), and an explicit integrability with paper based diagnostic platforms for point of care applications. These features empower the device with a favourable functionality in extremely challenging and resource limited settings in an ultra-low cost paradigm. As a consequence, the intrinsic porous capillaries in the paper structure drive a surface tension driven flow that induces ionic advection necessary for the establishment of an electrical potential across the device, resulting in a favourable direct exploitation and conversion of surface energy into electrical power.

We use standard laboratory grade filter paper (whatmann grade 1). We achieve to successfully harvest power of ~ 640 pW in single channel; which is further improved by O (~) 10^2 by connecting multiple channels (maximum up to 20 channels) through series connection. Our approach delineates a frugal, efficient and yet extremely robust platform for energy harvesting for sustained duration (up to 12 days) without requiring any sophisticated laboratory environment.

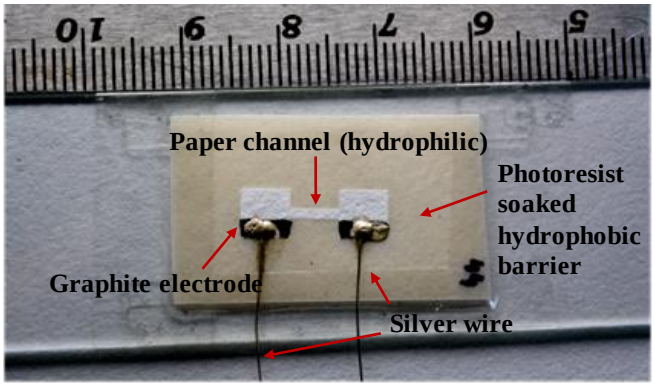

Figure 1: 'Paper-and-pencil'-based device used for streaming potential measurement. Device dimensions are 1 mm wide, 5 mm long with square inlet and outlet reservoir pads of 6mm × 6mm dimensions.

Experimental details

Chemicals

Potassium chloride (Merck Life Science Private Ltd.) and Whatman cellulose filter paper (GE Healthcare, UK) of grade 1 are used for the experimentation. Electrolyte solutions are prepared by mixing KCl in Milli Q deionized water (18MΩ cm).

Device fabrication

Paper channels are fabricated using photolithography technique similar to the process demonstrated by Mandal *et al*[43] (schematically delineated in Figure S1; see ESI). Hydrophobic coating of the paper leads to the blockage (evident from Figure S2; see ESI) of the paper pores and therefore the fabricated hydrophobic barrier guides the fluid transportation in definite direction. To fabricate the graphite electrodes, reservoir pads are sketched using HB pencil (Figure S2 in ESI). Silver wire (Sigma Aldrich: ≥99.99% trace metal basis, 1.59 μΩ-cm at 20°C) of ~250 μm diameter is attached to the pencil sketched electrodes using conductive silver paste (Alfa Aesar) for the measurement of the potential. To measure the streaming potential, Keithley 2182A nanovoltmeter is connected in parallel with the electrodes. Following the analogy of electrokinetics (i.e. the migration of counter ions in downstream direction), higher end of the nanovoltmeter probe is connected to downstream electrode (outlet reservoir pad) and the lower end is connected to the upstream electrode (inlet reservoir pad). In order to acquire the data continuously from nanovoltmeter, we use an in-house lab-view code. Details of the experimental and data measurement setup are schematically delineated in Figure 2. We use 1 mM KCl solution as the electrolyte throughout the entire course of investigation (for more details please see Figure S3 in ESI, where the effect of concentration on induced potential is shown). To eradicate the effect of evaporation, uniform experimental condition (relative humidity, RH: 50%, temperature: 22-24^{0}C) is maintained throughout the course of study.

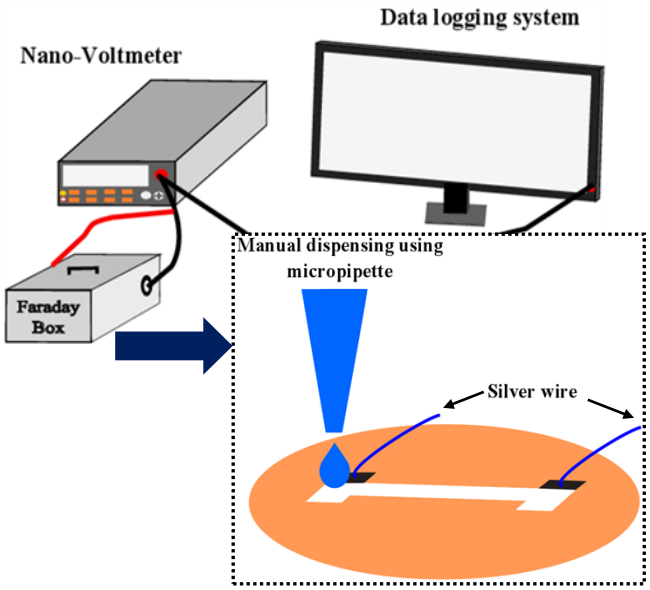

Figure 2: Schematic representation of the experimental setup for measuring streaming potential on 'paper-and-pencil' platform. Inset shows the inside view of Faraday box with manual dispensing of KCl solution on loading pad of the channel.

Equivalent electrical circuit

We exploit an analogy of equivalent electrical connection (shown in Figure 3) for continuous measurement of streaming

potential and output power. Paper channel (i.e. the hydrophilic part of the device) consists of numbers of micropores which can be assumed as an array of microchannels. We connect a nanovoltmeter in parallel with the electrodes to measure the open circuit potential. Further, an external resistance (R_L) is connected in parallel to the circuit to measure the respective close circuit potential. Inherent presence of the capillary force drives the electrolyte solution to the downstream direction through the micropores with resistance $R_{micropore}$. I_{str} is the streaming current that is being generated due to the advection of ions which develops an electrical field due to ion transportation and is known as streaming potential. This, in turn, induces the conduction current, I_c acting opposite to I_{str}. Thus the open circuit streaming potential for such a system can be calculated as[44]:

$$\Delta V_{stro} = Z\left(I_{str} - I_c\right)R_{micropore} \quad (1)$$

where, Z is the number of micropores within the channel area. However, in case of close circuit condition it can be calculated as,

$$\Delta V_{strc} = I_{ext}R_L \quad (2)$$

and $$I_{ext} = Z\left(I_{str} - I_c\right) \quad (3)$$

Now, the output power (P_{output}) can be calculated using the following formula:

$$P_{output} = \frac{(\Delta V_{strc})^2}{R_L} \quad (4).$$

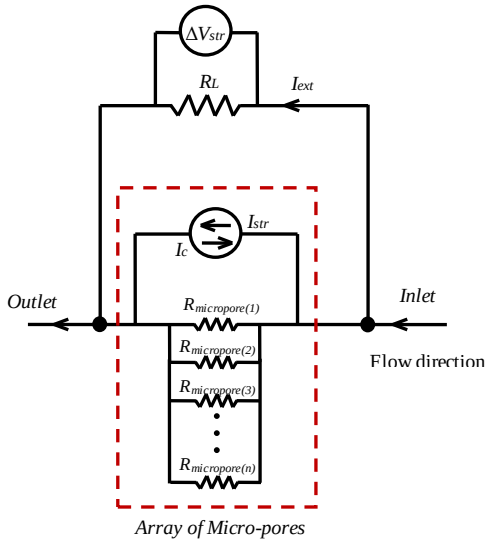

Figure 3: Schematic of equivalent electrical circuit used for streaming potential and output power measurement.

Results and discussions

Temporal variation of the induced open circuit potential is shown in Figure 4. Initial fluctuations can be ascribed to the fact of incomplete circuit (i.e. fluid is yet to reach to the outlet reservoir pad). Once the fluid makes contact with the outlet reservoir electrode, there is a sharp rise in the measured potential and thereafter it gradually decreases before it reaches a plateau regime.

Fundamental understanding about the microscopic structures of the paper and subsequent flow characteristics through such tortuous network is essential to explain the observed behavior of the streaming potential. Overall flow mechanism through paper-based microfluidic devices is fundamentally different from other conventional microfluidic platforms (glass, silicon, PDMS-based platforms). Due to the presence of inherent capillary action, fluid imbibes through the porous network of the paper matrix, not flowing on top of the surface. Paper is composed of enormous number of cellulose fabrics which are randomly distributed over the entire surface. Due to the presence of free carboxylic acid and hydroxyl groups, cellulose fibres are known to have free negative charges on its surface in contact with KCl solution, which is confirmed by the measured zeta potential (-8.76 ± 0.7813 mV)[45].

Therefore, due to the generation electrical double layer (EDL) on cellulose fabrics (effect of electrolyte's concentration is illustrated in Figure S3, please see ESI), there will be surplus of the counter ions in the downstream part of the channel (i.e. towards the direction of flow) which essentially leads to the generation of streaming potential across the two ends of the device (schematically shown in Figure 5). Interestingly, this occurs at virtually no expense, since the intrinsic porous capillaries in the paper structure essentially drive a surface tension driven flow that induces the advective transport of the ionic species for the establishment of the streaming potential, and no external pumping mechanism such as the syringe pump becomes necessary. Furthermore, the induced potential is certainly to be highest at the very initial phase i.e. when the circuit completes the connection for the first time and thereafter the potential is gradually decreasing. From Figure 4, it is clearly understood that at the very initial phase, the highest potential is measured which is continuously decreased with time and finally being stable for more than 2 hours; which indicates the fact that there is no more significant transportation of ions in macroscopic scale (i.e. in microscopic scale, ions are migrating in equivalent rate in almost all possible directions).

The temporal variation of induced potential for 1mM KCl solution is illustrated in Figure 4a (where DI water is used as a control experiment). From Figure S4 (in ESI), it can be inferred that the reproducibility of the measured results differs in different channels which can be accounted from the random distribution of the cellulose fabrics on the paper matrix. Further in Figure 4b, experimental reproducibility on the same channel is presented. Initial priming with KCl solution certainly decreases (as the micropores have already developed EDL) the initial fluctuation, whilst similar trend is observed for sustained period of measurement.

Following the results illustrated in Figure 4, it is clearly evident that the random distribution of cellulose network imparts some degree of fluctuation in measurements (particularly for longer period of the experiments). *In this context, one obvious concern arises what is the life span of the device?* To address this particular concern, we pay attention to understand the life cycle of the device. We perform a cyclic test which consists of 12 hours continuous measurement followed by ~10-12 hours of drying of the channel prior to the next cycle. The KCl solution (~50µl) is dispensed on the loading pad at an interval of one hour.

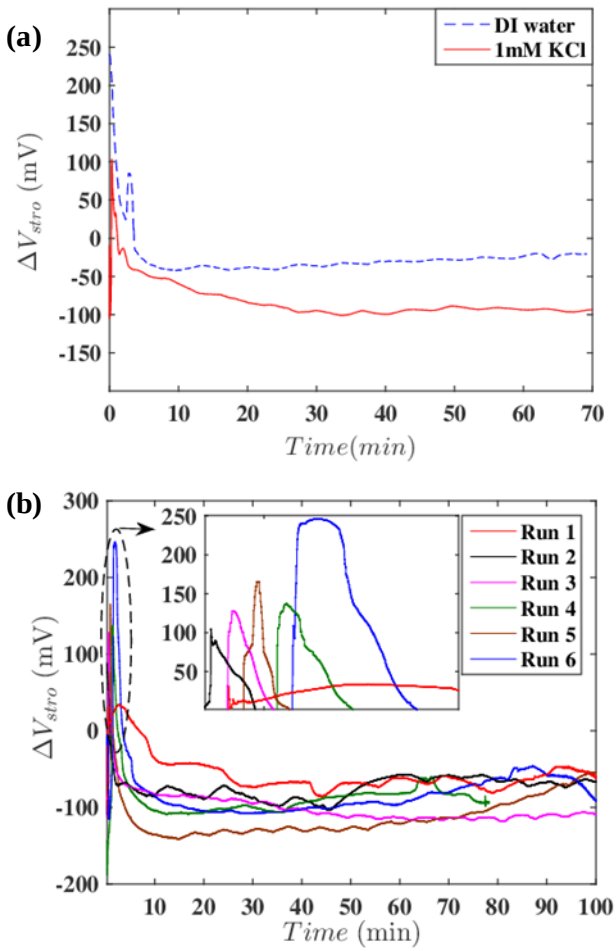

Figure 4: Temporal measurement of induced open circuit streaming potential for **(a)** 1mM KCl solution. DI water is used as a control study, **(b)** same channel for six consecutive runs (insets show the maximum open circuit potential in each run).

From Figure 6, three distinct regimes are observed. Regime 1 (R1) indicates the constant increase of performance rate of the device till ~60 hours, whereas the R2 indicates almost constant performance rate till ~100-110 hours; in R3 delineates attenuation of performance rate after 110 hours. The highest ΔV_{stro} (measured open circuit potential) obtained as ~-190mV at ~90 hours. So, it is important to note here that the device performance remains same even after ~140 hours of continuous operation; which is certainly an additional benefit for long term applications. Furthermore if we connect the nano-voltmeter probes in reverse connection mode (depicted in Figure S5, see ESI), polarity of the induced potential changes; which further confirms the effect of EDL on the observed phenomenon.

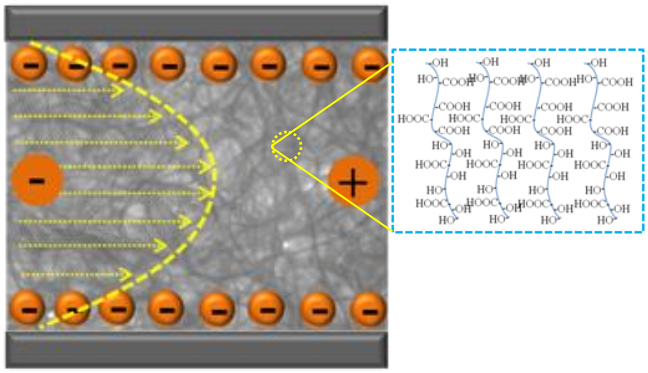

Figure 5: Schematic of the streaming potential generation on cellulose fibres (zoomed view: cellulose threads have –OH and –COOH functionality). Arrows indicate the direction of flow.

It is important to mention that Figure 6 indicates an augmentation in the device performance with number of usages, followed by a decrement beyond a critical usage. The possible reason of the observed trend in device performance may be owing to deposition of KCl on the cellulose fibres particularly due to the drying out of electrolyte solution. Due to crystallization of KCl on cellulose matrix (in case of repeated usage of the device), the effective pore size gets reduced. This, in turn, enhances the driving pressure gradient induced due to surface tension, which scales inversely with the pore radius. This can be realized from the increment of flow rate (Q) than initial runs (Q varies from 1-2.04µl/min in initial runs). Increase of flow velocity leads to the enhancement of advection current and hence higher induced streaming potential is seen. However, further increase of usage of the same device results in attenuation of the device performance. This can be explained by the fact that beyond certain number of usage leads to such an extent of KCl deposition which results in physical blockage of the pore to a considerable extent.

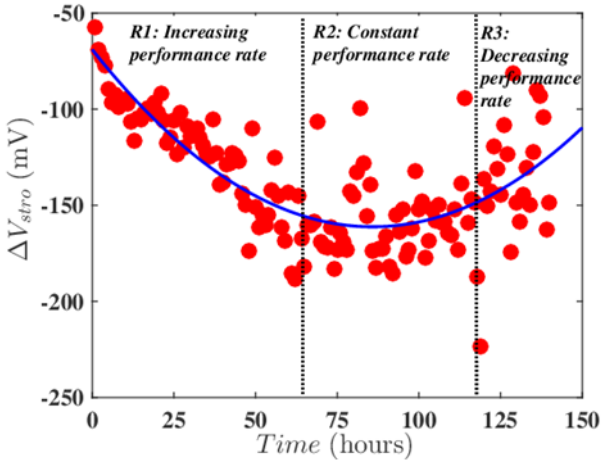

Figure 6: Cyclic test to investigate the performance of the paper channel with time.

In an effort to measure the closed circuit potential, an external load (R_L) is connected in parallel to the circuit. The variation of calculated output power agaisnt different load resistance is delineated in Figure 7. The maximum output power for single

channel is measured to be ~ 640 pW for the external resistance of 10 MΩ.

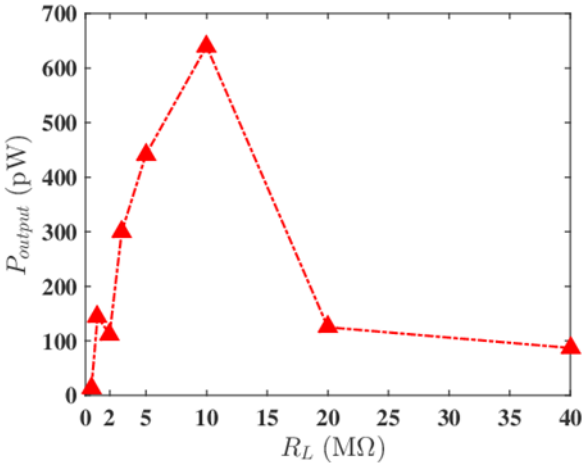

Figure 7: Variation of output power with respect to different load resistances (connected parallel to the circuit).

To realize the robustness of the device, it is very essential to perceive the role of relative humidity (RH) and temperature; which influence the evaporation rate, and hence the pumping power. To see the effect of temperature for a constant RH of ~50%, we systematically increase the temperature and observe that the streaming potential increases as we increase the temperature (shown in Figure 8). Under such scenario, device induces a maximum potential of ~180mV at 60°C. Increase in temperature increases the evaporation rate, and hence enhances the pumping rate to replenish the evaporative loss. This, in turn leads to higher induced potential. This may be exploited favourably in implementing the device in hot ambient (such as hot summer days) that intrinsically improves the device performance. Such hot ambience is common in field trials of point care diagnostic devices implemented in rural scenarios of the developing world. On the other hand, to investigate the effect of humidity, experiments are performed under a confinement where humidity is maintained during measurements. From Figure 9, it is evident that streaming potential decreases as the humidity of the surrounding environment increases. Increase in humidity reduces the evaporation rate which further decreases the induced streaming potential. We obtain maximum streaming potential of ~102mV at 50% RH (corresponding temperature is 24°C) and minimum streaming potential of ~6.6mV at 100% RH (corresponding temperature is 30°C). Therefore, the device can be very effective at hot and dry locations, which is a typical situation during the summer days in a vast part of the geographical world.

To further improve the output power, we connect the multiple channels (maximum up to 20 channels) through series connection (Figure S6 in ESI shows 5 channels; while the supplementary video shows a detailed measurement setup). Figure 10a shows that the maximum ΔV_{stro} observed is ~ 100mV for single channel, ~ 482mV for 5 channels, ~ 862mV for 10 channels and ~ 2.1V while 20 channels are in series connection.

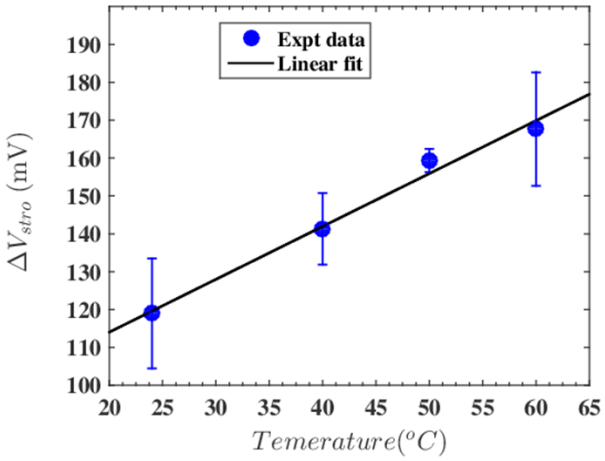

Figure 8: Induced open circuit streaming potential with respect to the different temperature conditions. The relative humidity of the ambient atmosphere is constant ~47-50%.

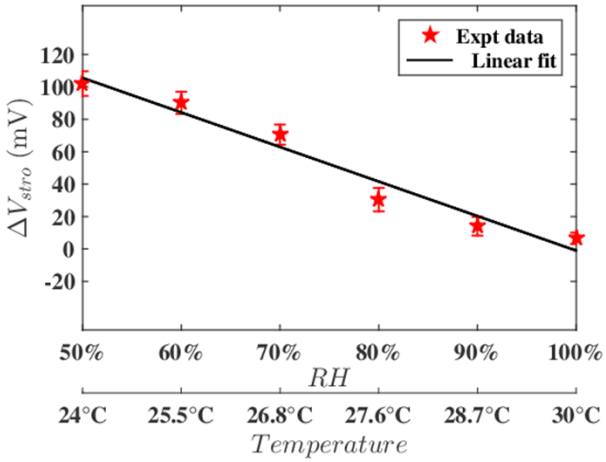

Figure 9: Induced open circuit streaming potential with respect to the different humidity and their corresponding temperature conditions.

In order to understand the device performance, the output power for single channel as well as for different channel combinations against different external loads is measured (depicted in Figure S7, see ESI). From this device optimization study, it is seen that for single channel maximum P_{Output} is seen against $10\,M\Omega$, whereas it is against $20\,M\Omega$, $40\,M\Omega$ and $80\,M\Omega$ for channel combination 5, 10, and 20 respectively. The temporal evolution of the output power for single channel and multiple channels (measured against the specific external load for which it shows maximum power) is seen to be almost constant as seen in Figure 10(b) for a period of 4 hours. Moreover, the device performance is seemed to be excellent till 12 days of measurements (see ESI, Figure S8); which indicates the robustness of the device.

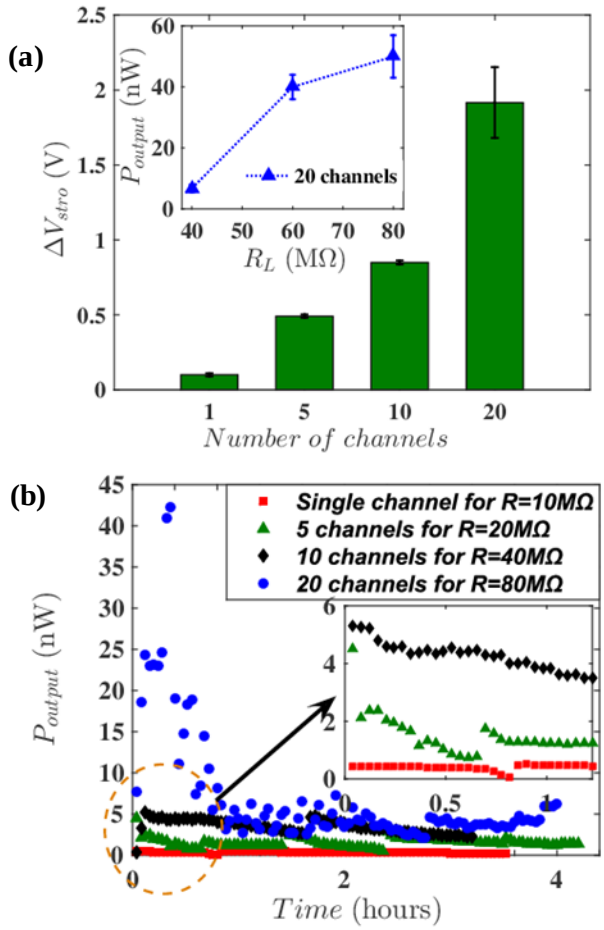

Figure 10: Variation of **(a)** open circuit potential for multichannel array shows the increase of open circuit potential as the number of channels in array is increasing from 1 to 5 to 10 to 20, (inset shows how the output power differs against different external load for 20 channels); and **(b)** temporal evolution of output power with respect to optimum external load resistance for multichannel array (inset indicates that at initial time points measured output power is higher while at later phase (~after 1 hour) it stabilizes to a constant potential value.

Furthermore, to develop a comprehensive understanding on the effect of the relevant geometrical parameters, we investigate the effect of channel dimensions (width and length) on the induced voltage. For a particular channel length (in our case 5mm), increase in channel width (W) leads to enhancement of generated potential (illustrated in Figure 11). Maximum streaming potential obtained for 3mm, 2mm and 1mm width channels are ~170mV, ~150mV and ~100mV respectively. Increment in width leads to the enhancement of capillary density which can be approximately estimated as $\sim W\Phi^{1/3}/D$, where W is the width of the paper channel, D is the pore diameter, Φ is the porosity of the paper[46]. Higher channel width (such as 3mm) corresponds to higher number of pores which resembles an array of micro-capillaries and thus induces higher streaming potential. Since the hydrophilic channel is surrounded by hydrophobic barrier, channel with lower width (such as 1mm) offers low flow rate due to flow retardation at the channel walls. However, in case of higher channel width the retardation effect from the hydrophobic barrier is no longer significant and thus flow rate increases and hence higher potential.

On the other hand, the effect of channel length (L) in Figure 12 illustrates that streaming potential increases as L increases till 10mm and then reduces with further increase in channel length. The highest average streaming potential obtained is ~175mV for L ~10mm channel. It is observed that for higher channel length, the rate of capillary filling decreases which subsequently leads to decrease of the potential value; while the capillary filling time does not get significantly affected between channel lengths 5-10 mm (capillary filling time for 5mm,10mm, 20mm and 30mm length channels are ~15-30 s, ~45-60 s, ~250-300 s, and ~ 540-585 s, respectively).

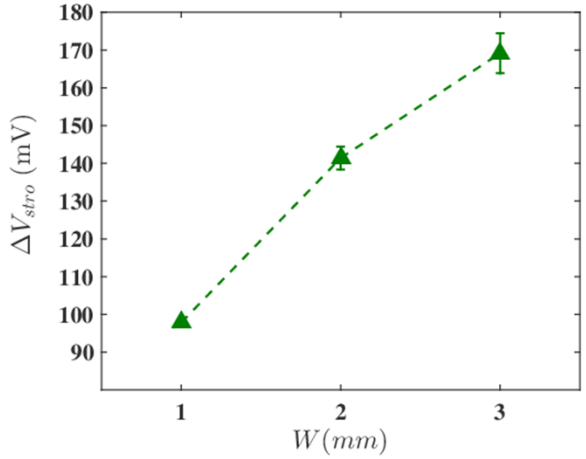

Figure 11: Variation of induced streaming potential with respect to the width of the channel. The length of the channel is 5mm.

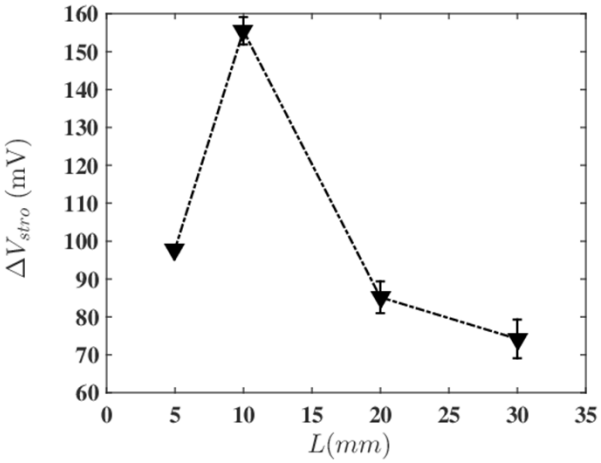

Figure 12: Variation of induced streaming potential with respect to the length of the channel. The width of the channel is 1mm.

To build a theoretical perspective for electrokinetic flows through a porous geometrical structure, such as a paper-based channel, here we make some assumptions to simplify the theoretical formalism without sacrificing the underlying physical principle. We assume that the porous structure of the paper is constructed of numerous micro-capillaries which are of cylindrical in shape having radii R (does not vary temporally), assumed to be arranged in parallel.

Due to the generation of EDL at the walls of these capillaries, ζ-potential of ψ_0 is developed. To obtain potential distribution (ψ) across such a single channel, one can employ the Poisson-Boltzmann equation[47]:

$$\frac{1}{r}\frac{d}{dr}\left(r\frac{d\psi}{dr}\right)=-\frac{ez\left(n_{+}-n_{-}\right)}{\varepsilon_0\varepsilon_r}=\frac{2ezn_0}{\varepsilon_0\varepsilon_r}\sinh\left(\frac{ez\psi}{k_BT}\right) \qquad (5)$$

Here, e is the protonic charge, z is the ionic valence (we consider z:z symmetry electrolyte for the analysis), $n_{\pm}$ is the number densities of cations and anions. Now, the electrolyte is transported through the micro-capillary due to a pressure gradient induced by the capillary action. Due to this transport, the total ionic current through a single capillary is given as:

$$I_{ionic}=ez\int\left(n_{+}u_{+}-n_{-}u_{-}\right)2\pi rdr \qquad (6)$$

where, $u_{\pm}$ is the velocity of cations and anions. For such a flow in the absence of any externally applied electric field, the total ionic current must vanish ($I_{ionic}=0$)[48] which leads us to the form of the induced streaming potential given as:

$$E_{str}=\frac{\frac{R\left(ze\right)^2\left(\sigma/L\right)}{\varepsilon_0\varepsilon_r\left(k_BT\right)^2}\int_0^R r\left(1-r^2/R^2\right)\psi dr}{\frac{\sigma\left(Rze\right)^2}{f\varepsilon_0\varepsilon_r\left(k_BT\right)}+\frac{\left(ze\right)^2\psi_0}{\left(k_BT\right)^2}\int_0^R 2\psi\left(1-\frac{\psi}{\psi_0}\right)rdr} \qquad (7)$$

(see ESI: section 9, for the complete derivation of Equation 7)

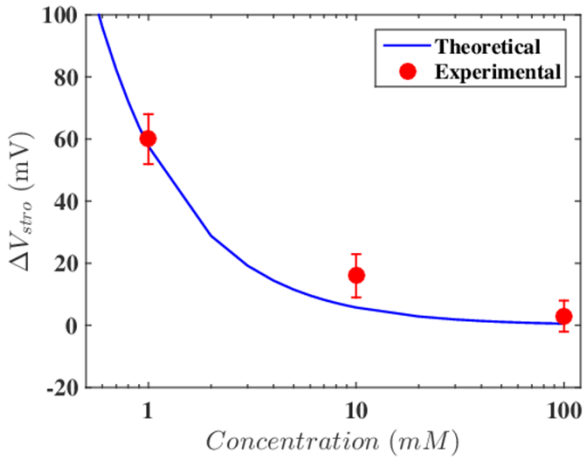

Figure 13: Variation of streaming potential with respect to electrolyte concentration (comparison between theoretical and experimental outcomes)

From Figure 13, it is evident that the theoretical predictions considering Equation (7) are quite well in agreement with our experimental findings. Observed minor deviations are attributable to the tortuous structure of the fiber matrix and alteration of the capillary diameter due to swelling etc, which are not trivial to consider from the perspective of mathematical modelling.

Prior to conclusion, it is important to summarize the key advantages of the present device as compared to the earlier reported works. Previously reported membrane based electrokinetc generator (which uses external energy for driving the flow through polymer membrane) provides an open circuit potential of ~3mV at 300kPa, power density of ~3.67W/m^2 and a conversion efficiency of ~46%[32]. This induced potential is in the expense of input energy (i.e. significant electrical power is required for pumping the liquid) while the output power is less as compared to its energy consumption. However, the present paper-pencil based energy harvesting device does not necessitate any external pumping power to drive the flow and entirely relies on capillarity coupled with natural evaporation for driving the liquid. Thus, the output electrical energy is harvested at the expense of intrinsic surface property of the device. It generates maximum open circuit potential of ~2.1V (for 20 array channels) as well as output power of ~50nW (for 20 array channels) which overweigh the corresponding values obtained from recently reported evaporation based electrokinetic energy generation devices (open circuit potential ~7mV and output power ~35nW)[34]. Moreover, the reported methods demand sophisticated fabrication techniques for fabrication of capillaries as well as for electrode implantation[34,35]; whereas, the present technique uses commonly available cellulose paper without necessitating any further surface treatment and simple pencil-sketched graphite electrode for harvesting electricity. The striking feature of the proposed technique is that a volume of 50µl KCl solution can generate power consistently more than ~1 hour. To further economize the device, photolithography technique for fabrication of paper channel can be substituted with simple printing-based technique as reported by Dey *et al.*[45]

Conclusions

In summary, a simple and frugal 'paper-and-pencil' based microfluidic array (on normal laboratory grade filter paper) has been demonstrated to be an efficient energy harvesting platform, having an inherent integrability with a corresponding analytical component (such as point of care diagnostics) of the same platform in an ultra-low cost paradigm. This virtually necessitates no input power that makes it potentially effective in challenging environments for point of care applications as hallmarked by resource-limited settings. The device essentially demonstrates a conceptualization of electrokinetics (streaming potential) in a paper based microfluidic platform, aided by an intrinsic surface tension driven connective transport of the ionic species through the porous network of the paper matrix. The device with single channel can develop maximum output power of ~640pW against external load of 10MΩ, whilst the maximum open circuit potential is observed as ~190mV. Multi-channel microfluidic arrays implemented on the same platform show substantial improvement in the measured output power (enhanced up to ~50nW by connecting 20 channels in series, for demonstration). Moreover, we perform comprehensive study to understand the optimized performance and robustness of the device. Cyclic test of the device revealed that ΔV_{stro} as well as the efficiency increases with the number of usages of the device and shows almost constant efficiency up to 12 days.

We envisage that these simple power generation platforms will find its application in the development of green battery, can further

be integrated power source for MEMS based low powering devices, and for self-powering paper-based medical diagnostic platforms that hold the potential of revolutionizing the implementation of point of care diagnostics in resource limited settings.

Acknowledgements

The authors would like to acknowledge Sponsored Research and Industrial Consultancy (SRIC) cell, IIT Kharagpur for the financial support to the 'Plant on-a-Chip' project provided through the SGDRI grant. SSD and SK would like to thank Dr. Jayabrata Dhar (postdoctoral fellow, Microfluidics Lab, IIT Kharagpur) for his assistance in developing the theoretical model.

Notes and references

1 X. Wang, J. A. Hagen, I. Papautsky, X. Wang, J. A. Hagen and I. Papautsky, *Biomicrofluidics*, 2013, **7**, 014107.

2 Z. Nie, C. A. Nijhuis, J. Gong, X. Chen, A. Kumachev, A. W. Martinez, M. Narovlyansky and G. M. Whitesides, *Lab Chip*, 2010, **10**, 477–483.

3 H. Hwang, S. Kim, T. Kim, J. Park and Y. Cho, *Lab Chip*, 2011, **11**, 3404–3406.

4 J. Hu, S. Q. Wang, L. Wang, F. Li, B. Pingguan-Murphy, T. J. Lu and F. Xu, *Biosens. Bioelectron.*, 2014, **54**, 585–597.

5 J. Noiphung, T. Songjaroen, W. Dungchai, C. S. Henry, O. Chailapakul and W. Laiwattanapaisal, *Anal. Chim. Acta*, 2013, **788**, 39–45.

6 A. W. Martinez, S. T. Phillips, M. J. Butte and G. M. Whitesides, *Angew. Chemie - Int. Ed.*, 2007, **46**, 1318–1320.

7 S. Kar, T. K. Maiti and S. Chakraborty, *Analyst*, 2015, **140**, 6473–6476.

8 L. J. Loh, G. C. Bandara, G. L. Weber and V. T. Remcho, *Analyst*, 2015, **140**, 5501–5507.

9 J. C. Jokerst, J. A. Adkins, B. Bisha, M. M. Mentele, L. D. Goodridge and C. S. Henry, *Anal. Chem.*, 2012, **84**, 2900–2907.

10 M. Zhang, L. Ge, S. Ge, M. Yan, J. Yu, J. Huang and S. Liu, *Biosens. Bioelectron.*, 2013, **41**, 544–550.

11 A. R. Rezk, A. Qi, J. R. Friend, W. H. Li and L. Y. Yeo, *Lab Chip*, 2012, **12**, 773–779.

12 D. Y. Kim and A. J. Steckl, *Appl.Mater.Inter.*, 2010, **2**, 3318-3323.

13 A. A. S. Jafarabadi-ashtiani, *Microfluid. Nanofluidics*, 2014, **16**, 989–995.

14 S. Kar, T. Kumar and S. Chakraborty, *Ina. Lett.*, 2016, **1**, 59–64.

15 S. Hu, R. Rajamani and X. Yu, *Appl. Phys. Lett.*, 2013, **104103**, 1–5.

16 A. C. Siegel, S. T. Phillips, M. D. Dickey, N. Lu, Z. Suo and G. M. Whitesides, *Adv. Funct. Mater.*, 2010, **20**, 28–35.

17 A. Russo, B. Y. Ahn, J. J. Adams, E. B. Duoss, J. T. Bernhard and J. A. Lewis, *Adv. Mater.*, 2011, **23**, 3426–3430.

18 M. Safdar, J. Jänis and S. Sánchez, *Lab Chip*, 2016, **16**, 2754–2758.

19 J. P. Esquivel, J. R. Buser, C. W. Lim, C. Domínguez, S. Rojas, P. Yager and N. Sabaté, *J. Power Sources*, 2017, **342**, 442–451.

20 Z. He, C. Zhong, S. Su, M. Xu, H. Wu and Y. Cao, *Nat. Photonics*, 2012, **6**, 591–595.

21 S. Mathew, A. Yella, P. Gao, R. Humphry-Baker, B. F. E. Curchod, N. Ashari-Astani, I. Tavernelli, U. Rothlisberger, M. K. Nazeeruddin and M. Grätzel, *Nat. Chem.*, 2014, **6**, 242–247.

22 J. S. Lim, Z. Abdul Manan, S. R. Wan Alwi and H. Hashim, *Renew. Sustain. Energy Rev.*, 2012, **16**, 3084–3094.

23 R. Veerubhotla, A. Bandopadhyay, D. Das and S. Chakraborty, *Lab Chip*, 2015, **15**, 2580–2583.

24 F. H. J. Van Der Heyden, D. J. Bonthuis, D. Stein, C. Meyer and C. Dekker, *Nano Lett.*, 2007, **7**, 1022–1025.

25 T. Nguyen, Y. Xie, L. J. de Vreede, A. van den Berg and J. C. T. Eijkel, *Lab Chip*, 2013, **13**, 3210.

26 A. Bandopadhyay and S. Chakraborty, *Appl. Phys. Lett.*, 2012, **101**, 043905.

27 C. Bakli and S. Chakraborty, *Electrophoresis*, 2015, **36**, 675–681.

28 D. Gillespie, *Nano Lett.*, 2012, **12**, 1410–1416.

29 Y. Xie, X. Wang, J. Xue, K. Jin, L. Chen and Y. Wang, *Appl. Phys. Lett.*, 2008, **93**, 8–11.

30 W. Guo, L. Cao, J. Xia, F. Q. Nie, M. Wen, J. Xue, Y. Song, D. Zhu, Y. Wang and L. Jiang, *Adv. Funct. Mater.*, 2010, **20**, 1339–1344.

31 F. H. J. Van Der Heyden, D. Stein and C. Dekker, *Phys. Rev. Lett.*, 2005, **95**, 9–12.

32 S. Haldrup, J. Catalano, M. R. Hansen, M. Wagner, G. V. Jensen, J. S. Pedersen and A. Bentien, *Nano Lett.*, 2015, **15**, 1158–1165.

33 A. Bentien, T. Okada and S. Kjelstrup, *J. Phys. Chem. C*, 2013, **117**, 1582–1588.

34 C. Li, K. Liu, H. Liu, B. Yang and X. Hu, *Mater. Res. Bull.*, 2017, **90**, 81–86.

35 G. Xue, Y. Xu, T. Ding, J. Li, J. Yin, W. Fei, Y. Cao, J. Yu, L. Yuan, L. Gong, J. Chen, S. Deng, J. Zhou and W. Guo, *Nat. Nanotechnol.*, 2017, **12**, 317–321.

36 D. D. Meng and C. C. J. Kim, *Lab Chip*, 2008, **8**, 958–968.

37 R. K. Arun, S. Halder, N. Chanda and S. Chakraborty, *Lab Chip*, 2014, **14**, 1661–1664.

38 N. K. Thom, K. Yeung, M. B. Pillion and S. T. Phillips, *Lab Chip*, 2012, **12**, 1768–1770.

39 H. Guo, M. H. Yeh, Y. Zi, Z. Wen, J. Chen, G. Liu, C. Hu and Z. L. Wang, *ACS Nano*, 2017, **11**, 4475–4482.

40 J. Wang, C. Wu, Y. Dai, Z. Zhao, A. Wang, T. Zhang and Z. L. Wang, *Nat. Commun.*, 2017, **8**, 1–7.

41 Y. Mao, N. Zhang, Y. Tang, M. Wang, M. Chao and E. Liang, *Nanoscale*, 2017, **9**, 14499–14505.

42 S. Jang, H. Kim and J. H. Oh, *Nanoscale*, 2017, **9**, 13034–13041.

43 P. Mandal, R. Dey and S. Chakraborty, *Lab Chip*, 2012, **12**, 4026.

44 K. Morikawa, K. Mawatari, M. Kato, T. Tsukahara and T.

Kitamori, *Lab Chip*, 2010, **10**, 871.

45 R. Dey, S. Kar and S. Joshi, T. K. Maiti and S. Chakraborty *Microfluid. Nanofluidics*, 2015, **19**, 375–383.

46 S. Hong and W. Kim, *Microfluid. Nanofluidics*, 2015, **19**, 845–853.

47 S. Das, S. Chanda, J. C. T. Eijkel, N. R. Tas, S. Chakraborty and S. K. Mitra, *Phys. Rev. E*, 2014, **90,** 043011.

48 A. Mansouri, C. Scheuerman, S. Bhattacharjee, D. Y. Kwok and L. W. Kostiuk, *J. Colloid Interface Sci.*, 2005, **292**, 567–580.